Journal of Solid State Chemistry 296 (2021) 121926

Contents lists available at ScienceDirect

Journal of Solid State Chemistry

journal homepage: www.elsevier.com/locate/jssc

Synthesis, structure, and properties of $EuScCuS_3$ and $SrScCuS_3$

Anna V. Ruseikina [a,*], Maxim S. Molokeev [b,c], Vladimir A. Chernyshev [d], Aleksandr S. Aleksandrovsky [b,c], Alexander S. Krylov [b], Svetlana N. Krylova [b], Dmitriy A. Velikanov [b], Maxim V. Grigoriev [a], Nikolai G. Maximov [e], Nikolai P. Shestakov [b], Alexander A. Garmonov [f], Alexey V. Matigorov [g], Anton S. Tarasov [b,c], Mikhail V. Rautskii [b], Nikolai A. Khritokhin [a], Ludmila V. Melnikova [h], Nikolay Yu Tretyakov [a]

[a] Institute of Chemistry, University of Tyumen, Tyumen, 625003, Russia
[b] Kirensky Institute of Physics, Federal Research Center KSC SB RAS, Krasnoyarsk, 660036, Russia
[c] Siberian Federal University, Krasnoyarsk, 660079, Russia
[d] Institute of Natural Sciences and Mathematics, Ural Federal University, Ekaterinburg, 620002, Russia
[e] Institute of Chemistry and Chemical Technology, Federal Research Center KSC SB RAS, Krasnoyarsk, 660049, Russia
[f] Institute of Physics and Technology, University of Tyumen, Tyumen, 625003, Russia
[g] Engineering Centre of Composite Materials Based on Tungsten Compounds and Rare-earth Elements, University of Tyumen, Tyumen, 625003, Russia
[h] University of Tyumen, Tyumen, 625003, Russia

ARTICLE INFO

Keywords:
Inorganic materials
Thermochemistry
Raman spectroscopy
Magnetic measurements
Optical spectroscopy
X-ray diffraction
Ab initio calculations

ABSTRACT

The crystal structures of the first-synthesized compound $EuScCuS_3$ and previously known $SrScCuS_3$ are refined by Rietveld analysis of X-ray powder diffraction data. The structures are found to belong to orthorhombic crystal system, space group *Cmcm*, structural type $KZrCuS_3$, with $a = 3.83413(3)$ Å, $b = 12.8625(1)$ Å, $c = 9.72654(8)$ Å ($SrScCuS_3$) and $a = 3.83066(8)$ Å, $b = 12.7721(3)$ Å, $c = 9.7297(2)$ Å ($EuScCuS_3$). The temperatures and enthalpies of incongruent melting are the following: $T_m = 1524.5$ K, $\Delta H_m = 21.6$ kJ•mol^{-1} ($SrScCuS_3$), and $T_m = 1531.6$ K, $\Delta H_m = 26.1$ kJ•mol^{-1} ($EuScCuS_3$). Ab initio calculations of the crystal structure and phonon spectrum of the compounds were performed. The types and wavenumbers of fundamental modes were determined and the involvement of ions participating in the IR and Raman modes was assessed. The experimental IR and Raman spectra were interpreted. $EuScCuS_3$ manifests a ferromagnetic transition at 6.4 K. The $SrScCuS_3$ compound is diamagnetic. The optical band gaps were found to be 1.63 eV ($EuScCuS_3$) and 2.24 eV ($SrScCuS_3$) from the diffuse reflectance spectra. The latter value is in good agreement with that calculated by the DFT method. The narrower band gap of $EuScCuS_3$ is explained by the presence of *4f-5d* transition in Eu^{2+} ion that indicates a possibility to control the band gap of the chalcogenides by the inclusion of Eu. The activation energy of crystal structure defects, being the source of additional absorption in the NIR spectral range, was found to be 0.29 eV.

1. Introduction

Ternary and quaternary semiconducting chalcogenide compounds $MCuX_2$ [1–13] and $MBCuX_4$ [14] (M = the third group elements, X = chalcogen, B = Sn, Ge) are being examined for decades. The chalcogenide compounds containing the third group elements can be used in electrooptics, photovoltaics, photodiodes, nonlinear optical devices, and absorbers in solar cells as well [15–19]. Several chalcogenides have rectilinear energy band gap approx. 1.2–1.5 eV [14] that is optimal for the solar cells and are the most prospective materials for the solar cell elements exhibiting about the 20% efficiency [3,8–10]. At present, little attention is paid to the preparation of complex chalcogenide compounds containing scandium [1,2,12,13] and to the investigation of their physical properties. Some works are related to triple compound $ScCuS_2$. This crystal is a semiconductor of *p*-type [1] with the specific electrical resistance of $2 \cdot 10^3$ Ω•cM [2]. According to the results of optical absorption analysis, it has energy band gap of 2.3 eV [2]. Then, by analogy with the compounds having isoformular composition [20], quaternary compounds $AScCuS_3$ can be formed in the $ScCuS_2$-AS (A = Eu, Sr) systems. $SrScCuS_3$ crystallizes in the orthorhombic space group *Cmcm* with the unit cell parameters $a = 3.8316(3)$, $b = 12.8504(9)$ and $c = 9.7153(7)$ Å [21]. However, in the literature, the data about synthesis and crystal

* Corresponding author. Institute of Chemistry, University of Tyumen, Perekopskaya 15a, Tyumen, 625003, Russia.
E-mail address: a.v.rusejkina@utmn.ru (A.V. Ruseikina).

https://doi.org/10.1016/j.jssc.2020.121926
Received 27 June 2020; Received in revised form 10 December 2020; Accepted 15 December 2020
Available online 5 January 2021

structure of $EuScCuS_3$, and properties of the $AScCuS_3$ (A = Sr, Eu) sulfides were not found. The presence of *d*- and *f*-elements in the crystal structure can provide a number of properties useful for different applications. The compounds $AScCuS_3$ (A = Sr, Eu) must be apparently related to the materials with good semiconducting *p*-type capability, the top of the valence band is composed of 3*d*-states of Cu, overlapped with 3*p*-states of S similarly to Cu_2S [22], and the materials $ACuX_2$ [1,23]. Synthesis of the compounds $ALnCuS_3$ is typically carried out by smelting of simple sulfides. However, the thermal dissociation of Sc_2S_3 appear at temperatures higher than 1100 °C [12], and, therefore, the synthesis of $AScCuS_3$ should be carried out at relatively low temperatures to maintain stoichiometric composition. The lack of data related to the properties of $AScCuS_3$ (A = Eu, Sr) limits the determination of the potential fields of their practical application.

The purpose of this research was to determine crystal structure, as well as thermal, optical, magnetic, and electrical properties of the compounds $AScCuS_3$ (A = Eu, Sr).

2. Experimental part

2.1. Materials

The following chemical reagents were used: Sc_2O_3 (99.9%, was procured in OOO SibMetalTorg, Russia), $SrCO_3$ (99.8%, was procured in VitaReactiv Company, Russia), Eu_2O_3 (99.9%, was procured by the manufacturers of Uralredmed, Russia), Cu (99.9%, was procured in SZBTsvetmet, Russia), argon (99.998% was procured in Kislorod-Servis – the manufacturer of technical gases, Russia), concentrated nitric acid (extra-pure grade, 18-4 all-Union State Standard 11125-84, Russia), ammonium rhodanide NH_4SCN (98%, was procured in Vekton Ltd., Russia).

2.2. Synthesis

The compounds of $EuScCuS_3$ и $SrScCuS_3$ in powdered form were prepared by the sulphidation of the oxide mixtures produced by thermolysis of the crystallized together metal nitrites [24,25]. The key steps of synthesis were similar for both compounds.

The metallic copper fragments were mechanically cleaned of oxide and basic-type carbonates formed in the air, then treated with alcohol and dried at room temperature (RT). Strontium carbonate and scandium oxide were desiccated at 570 K in a baker to remove sorption humidity of the materials. Europium oxide was annealed in a quartz beaker in an electric muffle at 1170 K for 2 h to remove hydroxides, hydrocarbonates and europium oxycarbonates, commonly formed in the rare-earth oxides of cerium subgroup [26–29]. We calculated the sample weights of the initial components by reference to the stoichiometric composition of $AScCuS_3$ (A = Sr, Eu).

For the preparation 10 g of $EuScCuS_3$, the weighed reagent batch was dissolved in 100 ml of 70% nitric acid being heated up to 330–350 K with constant stirring with magnetic bar stirrer [24]. In the preparation of $SrScCuS_3$, to solubilize $SrCO_3$, water was added in the ratio $1HNO_3{:}3H_2O$. This proportion results from the formation of the azeotropic mixture ($HNO_3{:}H_2O$) at the ratio of the reagents 1:3 [30] (eq. (1), (2)).

The nitrate solutions, containing cations Cu^{2+}, Sr^{2+}/Eu^{3+} and Sc^{3+}, were slowly evaporated at 350–360 K to dry residues and they were subjected to thermolysis at 830 K for 12 h. The mixture of the oxides obtained in the result of thermolysis was powdered and then sulfidized in the flow of H_2S and CS_2 produced by the decomposition of ammonium rhodanide (carrier gas is argon) [24,31]. The sulfidization was carried out in three stages: at 870 K for 6 h, at 1070 K for 4 h and at 1170 K for 15 h. The compounds $AScCuS_3$ (A = Eu, Sr) were obtained in a powder form. $EuScCuS_3$ is black, and $SrScCuS_3$ is yellow-brown.

2.3. Methods

The powder diffraction data of $AScCuS_3$ (A = Eu, Sr) for Rietveld analysis were collected at RT with a Bruker D8 ADVANCE powder diffractometer (Cu-Kα radiation) and linear VANTEC detector. The step size of 2θ was 0.02°, and the counting time was 13 s ($SrScCuS_3$) and 26 s ($EuScCuS_3$) per step. Although the structure of $SrScCuS_3$ has already been known, it was decided to refine it according to Rietveld in order to 1) prove its chemical composition, phase purity of powder, that is important to physical measurements (Raman spectroscopy, IR-spectroscopy, thermal properties, etc); 2) obtain crystal structures of $AScCuS_3$ (A = Eu, Sr) using one and the same method and device for correct comparison of all calculated values, using structural information. The unit cell parameters were determined with the use of ITO program [32]. The observed systematic absences showed that the $AScCuS_3$ (A = Eu, Sr) structure belongs to space group *Cmcm* (for hkl: h + k = 2n; for 0 kl: k = 2n; for h0l: h, l = 2n; for h00: h = 2n; for 0k0: k = 2n, and for 00l: l = 2n). The Rietveld refinement was performed by using TOPAS 4.2 package [33]. The initial model is used as the dataset for the isostructural compound $SrLuCuS_3$ [34,35]. The Lu ion was replaced by Sc ion. The thermal parameters of Sr and Eu ions were refined anisotropically, and thermal parameters of all the other ions isotropically. Apart from the major phase, the refined model included identified micro impurities: 1.27(7) wt. % SrS (SrScCuS$_3$). Refinements were stable and gave low R-factors (for $SrScCuS_3$: $R_{wp} = 3.77\%$, $R_p = 2.97\%$, $R_{exp} = 2.61\%$, $\chi^2 = 1.448$, $R_B = 1.45\%$; for $EuScCuS_3$: $R_{wp} = 4.08\%$, $R_p = 3.12\%$, $R_{exp} = 2.61\%$, $\chi^2 = 1.56$, $R_B = 1.62\%$). The crystallographic data of $EuScCuS_3$, which are new, were deposited in Cambridge Crystallographic Data Center (CCDC #2000584). The data can be downloaded from the site (www.ccdc.cam.ac.uk/data_request/cif). Crystal structures were visualized in the program package Diamond 3 [36].

The ab initio calculations of the crystal structure and phonon spectrum of $SrScCuS_3$ and $EuScCuS_3$ were carried out in the framework of density functional theory (DFT) [37] using the B3LYP exchange-correlation functional [38,39], which takes into account both local and nonlocal Hartree−Fock exchanges. The calculations were carried out in the program CRYSTAL17 [40,41]. For europium, the ECP53MWB quasi-relativistic pseudo-potential [42,43] was used with the attached valence basis set ECP53MWB [44]. The Gaussian primitives with exponents less than 0.1 were removed from the basis sets. The exponent in the outer *d*-orbital of the valence basis set was set to 0.279. For copper, the full-electron basis set [45] was used, as available on the CRYSTAL program site « Cu_86–4111(41D)G_doll_2000» [41]. For sulfur, the DURAND pseudo-potential with the attached valence basis set was used [41,46]. The exponents in the two outer orbitals of the valence basis set were set to 0.18 and 0.24. For strontium, the ECP28MWB quasi-relativistic pseudo-potential [47] was used with the attached valence basis set ECP28MWB [44]. The Gaussian primitives with exponents less than 0.1 were removed from the basis sets as well. The exponents in the two outer *p*- and *d*- orbitals of the valence basis set were set to 0.181 and 0.118, respectively. For scandium, the pseudo-potential HAYWSC [48] was used, as available on the CRYSTAL program site « Sc_HAYWSC-311d31_bredow_2006» [41]. 105 IBZ points were used. The

$$SrCO_3 + Sc_2O_3 + Cu + 12HNO_3 \rightarrow Sr(NO_3)_2 + 2Sc(NO_3)_3 + Cu(NO_3)_2 + 6H_2O + 2NO_2\uparrow + CO_2\uparrow \quad (1)$$

$$Sc_2O_3 + Eu_2O_3 + Cu + 16HNO_3 \rightarrow 2Sc(NO_3)_3 + 2Eu(NO_3)_3 + Cu(NO_3)_2 + 8H_2O + 2NO_2\uparrow \quad (2)$$

Scheme 1. Dissolution of the initial components.

use of pseudo-potentials for the description of core electronic shells of rare-earth ions, the 4*f* inclusive, with the basic valence sets for outer orbitals involved in chemical bonding, makes it possible to successfully reconstitute the lattice structure and lattice dynamics in the compounds that have a lanthanide ion sublattice [49,50]. The accuracy of self-consistently solving of the system of Kohn-Sham equations was set at 10-10 a.u. The accuracy of the calculation of the two-electron integrals was set no less than 10-8 a.u. The Monkhorst-Pack shrinking factor was taken to be 8 × 8 × 8, which corresponded to 105 IBZ points. The phonon spectrum was calculated in the harmonic approximation. In the Hessian matrix, the first (second) derivatives were calculated analytically (numerically). At numerical calculations of the second derivatives, the atom was displaced from the equilibrium position by 0.003 Å. The crystal structure was calculated at first, followed by phonon spectrum calculations based on the optimal crystal structure. The calculation details can be found elsewhere [49].

The infrared absorption spectra were recorded in the range of 680–85 cm^{-1} using an FTIR VERTEX 80V spectrometer (BRUKER OPTIK GMBH) equipped by an RT-DTGS FIR sensor. Powders of the sulfides under investigation were grinded in an agate mortar and then were mixed with ultrahigh molecular weight polyethylene (Mitsui Petrochemical Ind., Japan) in a ratio of 1:10 and pressed into 0.26 mm thick pellets.

The experimental Raman spectra of $EuScCuS_3$ and $SrScCuS_3$ compounds were collected in backscattering geometry, using a triple monochromator JobinYvon T64000 Raman spectrometer operating in subtractive mode then detected by a liquid nitrogen-cooled CCD cooled at 140 K. The spectral resolution for the recorded Stokes side Raman spectra was better than 1 cm^{-1} (this resolution was achieved by using gratings with 1800 grooves mm^{-1} and 100 μm slits). The single-mode radiation at 647.09 nm from Lexel Kr^+ was used as an excitation light source, power on the sample being 5 mW.

Scanning electron microscopy (SEM) was performed on a JEOLJSM-6510 LV equipped with an energy dispersive spectrometer.

The four-contact probe method was used for the transport properties studies. The powder samples were pounded with a pestle in an agate mortar and pressed at 1.25 GPa for 2 min using an automatic hydraulic press Specac Atlas 40 t to form a tablet with a diameter of 20 mm and 0.3 mm thick.

The silver epoxy conductive contacts were placed on top of prepared samples to measure electrical resistance. During the measurements, the samples were cooled down to 77 K and heated to 295 K in the home-made setup consisted of flow cryostat, an electromagnet and Source Meter 2634B (Keithley) [51].

The differential scanning calorimetry experiments were carried out on a Setsys Evolution 1750 (TG–DSC 1600) with the aid of the PtRh 6%-PtRh 30% thermocouple. The device was calibrated according to the data of melting temperatures and melting enthalpies of standard substances (Sn, Pb, Zn, Al, Ag, Au, Cu, and Pd). Prior to an experiment, the working chamber of the device was evacuated and then filled with argon. The recording parameters were the following: the sample size: 100–110 mg, argon flow rate: 25 ml·min^{-1}, and alundum crucible capacity: 100 μl. The differential thermal dependency characteristic curves were processed in the programming complex Setsoft Software 2000. According to TG curves, no weight loss was observed. The kinetic parameters of incongruent melting of the $AScCuS_3$ (A = Eu, Sr) compounds were determined at different rates of heating: 5, 7, 10, 15 K·min^{-1}. The kinetic parameters determination was based on Kissinger formula [52] in the linearized form (eq. (3)):

$$\frac{1}{T} = \frac{R}{E} ln \frac{b}{T^2} - \frac{R}{E} ln \frac{AR}{E} \quad (1)$$

where T is the temperature with maximum reaction rate; b – the heating rate, K·c^{-1}; E – activation energy; A - preexponential factor; R is the gas constant (8.314 J·mol^{-1} K^{-1}).

The $EuScCuS_3$ sample 62.0 mg in mass was studied on a SQUID magnetometer [53] in the 10 Oe (796 A·m^{-1}) magnetic field. The measurements of low-temperature magnetization were performed in the ZFC (zero-field cooled) and FC (nonzero-field cooled) modes. The powder sample of $SrScCuS_3$ was tightly packed into the polyvinylchloride container with the lid (4.2 mm in diameter and 5.8 mm high). The mass of the sample was 58.0 mg. The room-temperature magnetic properties of $SrScCuS_3$ were studied on a vibrating sample magnetometer with a Puzey electromagnet [54]. The magnetic field was varied in 20–100 Oe (1.59–7.96 kA·m^{-1}) steps. The magnetometer signal from the container and the lid were measured separately and then subtracted from the whole signal. The samples were weighed by means of an analytical balance Mettler Toledo ME204 within the accuracy of 0.1 mg.

The diffuse reflection spectra of $SrScCuS_3$ and $EuScCuS_3$ were measured using a Shimadzu UV-3600 spectrometer. DR measurements were done from 220 nm to 1400 nm.

3. Results and discussion

3.1. Crystal structure

The $SrScCuS_3$ and $EuScCuS_3$ diffraction patterns were indexed in terms of orthorhombic space group *Cmcm*, $KZrCuS_3$ structural type, with the unit cell parameters: a = 3.83413(3) Å, b = 12.8625(1) Å, c = 9.72654(8) Å; V = 479.680(7) $Å^3$, Z = 4, ρ_x = 4.042 g·cm^{-3} ($SrScCuS_3$) and a = 3.83066(8) Å, b = 12.7721(3) Å, c = 9.7297(2) Å; V = 476.029(17) $Å^3$, Z = 4, ρ_x = 4.977 g·cm^{-3} ($EuScCuS_3$) (Fig. 1).

The unit cell parameters calculated in the DFT framework with the B3LYP functional (a = 3.826 Å, b = 12.776 Å, c = 9.747 Å, V = 476.396 $Å^3$, ρ_x = 4.067 g·cm^{-3} for $SrScCuS_3$ and a = 3.807 Å, b = 12.833 Å, c = 9.679 Å, V = 472.815 $Å^3$, ρ_x = 5.011 g·cm^{-3} for $EuScCuS_3$ accordingly) correlate with the experimental values.

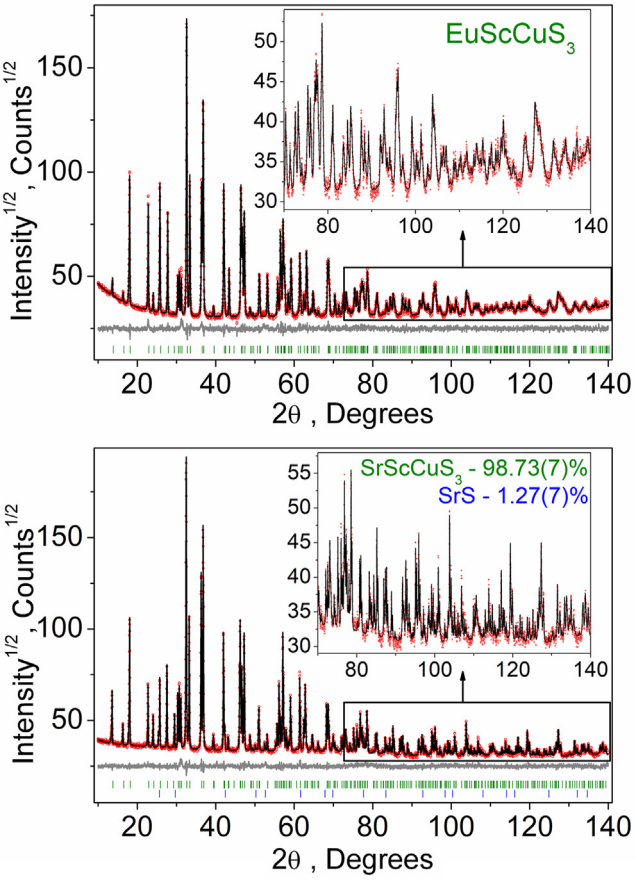

Fig. 1. Difference Rietveld plot of $EuScCuS_3$ and $SrScCuS_3$. The bars indicate the peak positions of the major phase and SrS.

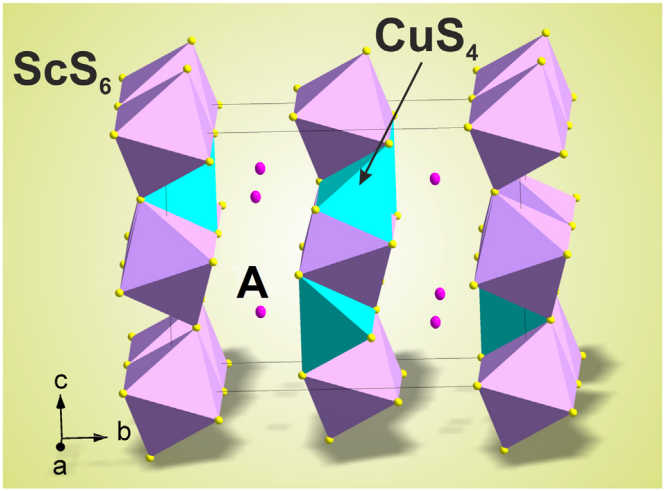

Fig. 2. Crystal structure of $AScCuS_3$ (A = Sr, Eu). The ellipsoids are drawn at the 50% probability level.

Table 1
Fractional atomic coordinates and isotropic displacement parameters ($Å^2$) of $EuScCuS_3$.

Atom	Wyck.	Site	*x*	*y*	*z*	B_{iso}*/B_{eq}
Eu	4c	m2m	0	0.74739 (8)	0.25	0.93 (4)
Cu	4c	m2m	0	0.53034 (14)	0.75	1.23 (7)*
Sc	4a	2 m.	0	0	0	0.50 (6)*
S1	8f	m.	0	0.36450 (17)	0.0571 (2)	0.80 (7)*
S2	4c	m2m	0	0.0755 (2)	0.25	1.01 (9)*

Table 2
Interatomic distances (*d*) and their average values in the $EuScCuS_3$ structure.

Bond	*d*, Å	Bond	*d*, Å	Bond	*d*, Å
Eu—S1^{i}	3.0705 (17) (×4)	Sc—S1^{iv}	2.6405 (15) (×4)	Cu—S1^{ii}	2.3079 (23) (×2)
Eu—S2^{i}	2.9134 (23) (×2)	Sc—S2	2.6166 (10) (×2)	Cu—S2^{iii}	2.3444 (19) (×2)
<Eu—S>	3.02(8)[a]	<Sc—S>	2.63(1)[a]	<Cu—S>	2.33(3)[a]

[(a)] Regular variations of distances due to the polyhedral distortion [63]. Symmetry codes: (i) -*x*+1/2, *y*+1/2, -*z*+1/2; (ii) -*x*, -*y*+1, -*z*+1; (iii) -*x*+1/2, -*y*+1/2, -*z*+1; (iv) -*x*+1/2, -*y*+1/2, -*z*.

The structure of the compounds $AScCuS_3$ (A = Sr, Eu) is described by the 2D layer [$ScCuS_3$] in coplanarity *a*-*c*, formed by distorted tetrahedrons of CuS_4 and octahedrons of ScS_6, with the ions of Sr^{2+} or Eu^{2+} ions located between the layers (Fig. 2). The atomic coordinates and selected interatomic distances for $SrScCuS_3$ are reported in Supporting Information (Table S1, Table S2) and for $EuScCuS_3$ (Table 1, Table 2).

The crystal structures $AScCuS_3$ (A = Sr, Eu) are isostructural and their structural parameters are close to each other due to small difference of ion radii $r_{Sr^{2+}}$ = 1.18 Å and $r_{Eu^{2+}}$ = 1.17 Å (CN = 6) [55]. Differences in the values of the ionic radii Sr^{2+}/Eu^{2+} and Sc^{3+} are considerable and reach to Δ*r*(Sr–Sc) = 36.9% ($r_{Sc^{3+}}$ = 0.745 Å, CN = 6 [54]), Δ*r*(Eu–Sc) = 36.3%. That is probably why the ions Sr^{2+}/Eu^{2+} and Sc^{3+} take up two independent crystallographic positions as distinct from isomorphous compounds $ALnCuS_3$ (Ln = La–Nd [35,56]) with light rare-earth elements where Sr^{2+}/Eu^{2+} and Ln^{3+} take up one position at subtle differences in ionic radii Δr(Sr–La) = 9.1%, Δr(Eu–La) = 8.3% ($r_{Eu^{2+}}$ = 1.20 Å, $r_{Sr^{2+}}$ = 1.21 Å,$r_{La^{3+}}$ = 1.10 Å, CN = 7 [55]). Higher values of bonding distances dSr-S (Table S2), as compared to dEu-S, are related to the principally different electronic structure of the ions Sr^{2+} и Eu^{2+}. Thus, the compound $SrScCuS_3$ is characterized by higher ionic bond character than $EuScCuS_3$. This is compliant with the observation that alkaline elements have more distinct ionic characteristic in comparison to rare-earth metals [57]. In the compounds $EuScCuS_3$ и $SrScCuS_3$ the ions of Eu^{2+} and Sr^{2+} have similar coordination numbers, but different coordination polyhedra. This may be associated with the fact that the compound, containing more ionic polyhedron SrS_6, is characterized by highly symmetrical coordination, and less ionic polyhedron EuS_6 is specified by less symmetrical trigonal-prysmatical coordination.

In the isostructural compounds $AScCuS_3$ (A = Ba, Sr, Eu), thinning of the radius of the divalent ion $r_{Ba^{2+}}$ = 1.35 Å [55] > $r_{Sr^{2+}} > r_{Eu^{2+}}$ results in the decrease of the cell parameters and cell volume: *V* = 513 $Å^3$ ($BaScCuS_3$ [57]) → 479.680(7) $Å^3$ ($SrScCuS_3$) → 476.029(17) $Å^3$ ($EuScCuS_3$).

In the previously examined compounds of $EuLnCuS_3$ europium is divalent [58–61]. The insignificant structural difference anticipates similarity of charges in the compounds $AScCuS_3$ (A = Sr, Eu) as well. The bond valence sum calculation is frequently used for the determination of valence states from the XRD data. According to the bond valence sum calculations: Val_{Eu} = 1.90, Val_{Sc} = 2.59, Val_{Cu} = 1.26 ($EuScCuS_3$); Val_{Sr} = 1.77, Val_{Sc} = 2.65, Val_{Cu} = 1.28 ($SrScCuS_3$) with the parameters outlined in Ref. [62], and the valence states of Eu(Sr), Sc and Cu ions in $ALnCuS_3$ are close to 2, 3 and 1, respectively.

The powdered compounds $AScCuS_3$ (A = Eu, Sr) consist of particles with linear sizes up to 10–20 μm (Fig. 3). The energy dispersive X-ray spectrometric analysis was performed at five different locations on the sample surface. According to the data of energy dispersive X-ray spectrometric analysis, the ratio of the elements is m_{found}(Eu) = 42.8 (9) mass. %, m_{found}(Sc) = 12.6 (3) mass.%; m_{found}(Cu) = 17.9 (4) mass.%; m_{found}(S) = 26.7 (5) mass.% and m_{found}(Sr) = 30.8 (6) mass.%; m_{found}(Sc) = 15.2 (3) mass.%; m_{found}(Cu) = 21.5 (4) mass.%; m_{found}(S) = 32.5 (6) mass.%, respectively. The chemical compositions of the samples are compliant with the theoretical contents of the elements and the X-ray diffraction analysis data.

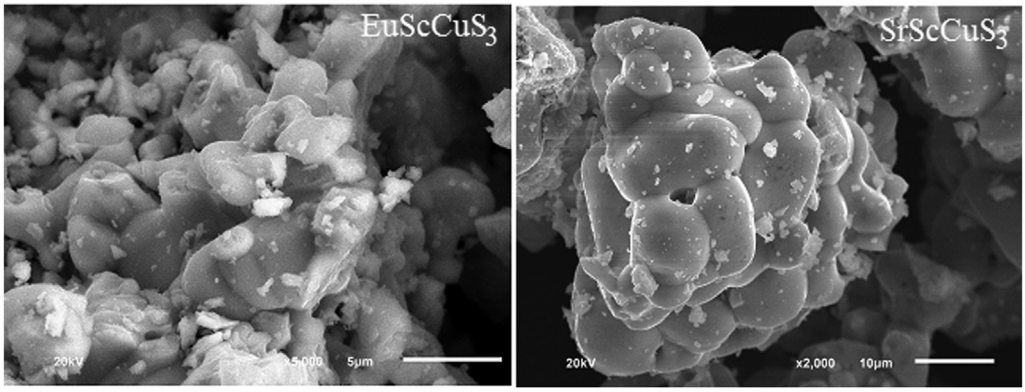

Fig. 3. The SEM patterns of the $SrScCuS_3$ (A = Eu, Sr) samples.

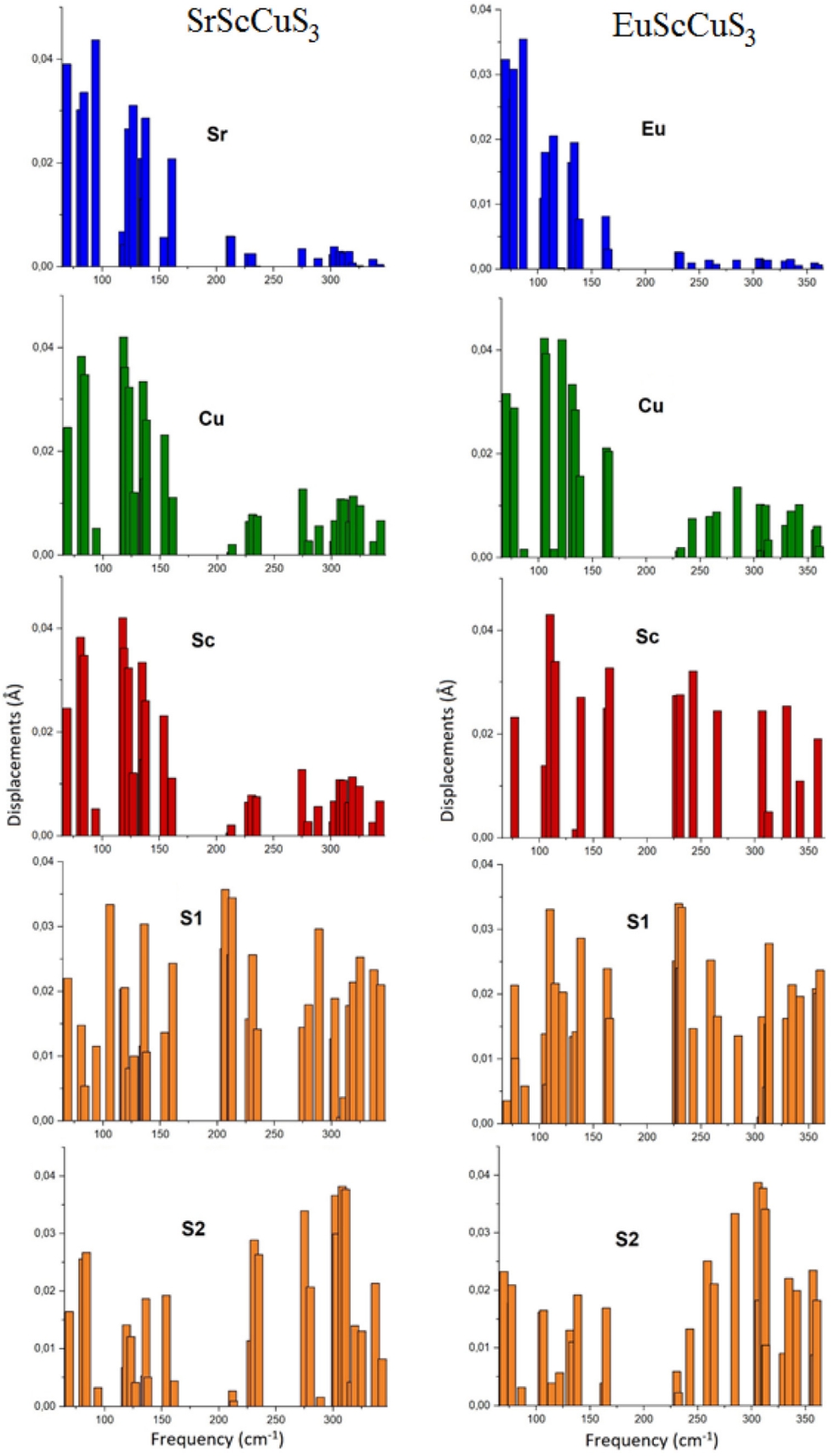

Fig. 4. The displacements of ions at phonon modes.

Table 3
Irreducible representations, classification of modes, and Raman tensors for $EuScCuS_3$ and $SrScCuS_3$ (space group *Cmcm*, N° 63).

Atom	Phonon modes at point G
Eu (Sr)	$A_g + B_{1g} + B_{3g} + B_{1u} + B_{2u} + B_{3u}$
Cu	$A_g + B_{1g} + B_{3g} + B_{1u} + B_{2u} + B_{3u}$
Sc	$2B_{1u}+2B_{2u} + B_{3u} + A_{1u}$
S1	$2A_g + B_{1g} + B_{2g}+2B_{3g}+2B_{1u}+2B_{2u} + B_{3u} + A_{1u}$
S2	$A_g + B_{1g} + B_{3g} + B_{1u} + B_{2u} + B_{3u}$
Classification of modes	
$M = 5A_g + 2A_u + 4B_{1g} + 7B_{1u} + B_{2g} + 7B_{2u} + 5B_{3g} + 5B_{3u}$ $\Gamma_{acoustic} = B_{1u} + B_{2u} + B_{3u}$ $\Gamma_{IR} = 6B_{1u} + 6B_{2u} + 4B_{3u}$ $\Gamma_{Ram} = 5A_g + 4B_{1g} + B_{2g} + 5B_{3g}$	

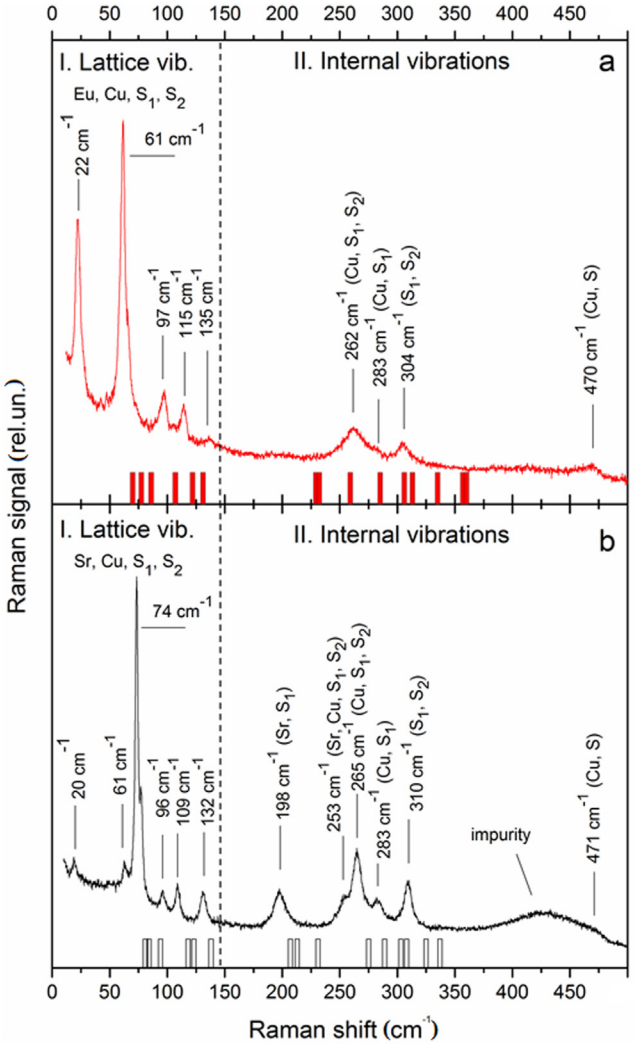

Fig. 5. Raman experimental and calculated spectra of the compounds: a) $EuScCuS_3$, b) $SrScCuS_3$.

3.2. Ab initio lattice dynamics calculations and the interpretation of observed vibrational spectra

The types of phonon modes in $SrScCuS_3$ and $EuScCuS_3$ were determined, and the involvement of ions in vibrational modes was evaluated on the basis of the displacement vectors derived by ab initio calculations (Fig. 4, Tables S3–S5). In the IR spectrum (Table S3), strontium (europium) ions are appreciably involved in low-wavenumber modes. The strontium ions are involved in the modes with wavenumbers up to 160 cm^{-1}. The europium ions are involved in the modes with wavenumbers up to 130 cm^{-1}. The greatest involvement of strontium (europium) is predicted at the low-wavenumber mode 69 (76.9) cm^{-1} (B_{1u}). The copper ion vibrations appear in the IR modes with wavenumbers of up to 165 cm^{-1} and at the mode B_{2u} with wavenumber 311 cm^{-1} as well. The greatest involvement of copper is in the 69 cm^{-1} (B_{1u}), 119 cm^{-1} (B_{2u}), 135 cm^{-1} (B_{3u}) and 154 cm^{-1} (B_{1u}) modes at $SrScCuS_3$. The greatest involvement of copper is in the 76.9 cm^{-1} (B_{1u}), 105 cm^{-1} (B_{2u}), 134 cm^{-1} (B_{3u}), 163 cm^{-1} (B_{3u}) and 165 cm^{-1} (B_{1u}) modes at $EuScCuS_3$. Scandium vibrations appear in the IR modes with wavenumbers of up to 280 cm^{-1} and at the three high-wavenumber modes 316 cm^{-1} (B_{3u}), 319 cm^{-1} (B_{1u}), 343 cm^{-1} (B_{3u}) at the $SrScCuS_3$. Scandium vibrations appear in the IR modes with wavenumbers of up to 307 cm^{-1} and at the three high-wavenumber modes 330 cm^{-1} (B_{3u}), 342 cm^{-1} (B_{1u}), 359 cm^{-1} (B_{3u}) at the $EuScCuS_3$. Sulfur is involved in all IR modes. Sulfur S2 and scandium are strongly involved in the most intensive B_{1u} mode (235 and 265 cm^{-1} in $SrScCuS_3$ and $EuScCuS_3$, respectively). Sulfur S1 and scandium are strongly involved in the most intensive B_{2u} mode (212 and 230 cm^{-1} in $SrScCuS_3$ and $EuScCuS_3$, respectively).

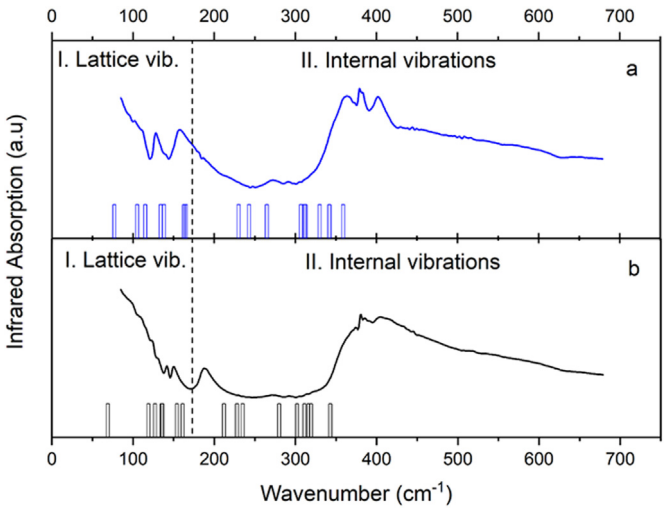

Fig. 6. Infrared experimental and calculated spectra of the compounds: a) $EuScCuS_3$, b) $SrScCuS_3$.

Each mode involves several ions of different types. For example, the low-wavenumber IR mode (B_{1u} 62 cm^{-1} and B_{1u} 76.9 cm^{-1}) involves all ions (Sr (Eu), Cu, Sc, and S), and it is difficult to distinguish the dominant contribution from any one of them.

According to the calculations, strontium (europium) is involved in the Raman modes (Table S4) with wavenumbers up to 161 (163) cm^{-1}. In $SrScCuS_3$, the copper vibrations appear in the Raman modes with wavenumbers up to 138 cm^{-1} and in the modes at 275 cm^{-1} (A_{1g}), 308 cm^{-1} (B_{1g}) and 325 cm^{-1} (B_{2g}). In $EuScCuS_3$, the copper vibrations appear in the modes with wavenumbers up to 131 cm^{-1} and in the modes at 285 cm^{-1} (A_g), 306 cm^{-1} (B_{1g}) and 335 cm^{-1} (B_{2g}). Strontium is not involved in Raman modes. Sulfur is involved in all Raman modes. Only sulfur ions S1 participate in the B_{3g} mode at 207 cm^{-1} (229 cm^{-1} in $EuScCuS_3$). The predominant participation of sulfur S1 is found in mode B_{1g} with wavenumber 213 cm^{-1} (232 cm^{-1} in $EuScCuS_3$). The sulfur ions predominantly participate in the most intensive A_g mode (337 cm^{-1} in $SrScCuS_3$ and 360 cm^{-1} in $EuScCuS_3$).

The A_u modes, which are IR- and Raman-inactive, were also obtained by the calculations (Table S5). Scandium and sulfur S1 are strongly involved in these mods.

From the analysis of displacement vectors obtained from the ab initio calculations, the each ion participation degree was estimated for a particular mode (Fig. 4).

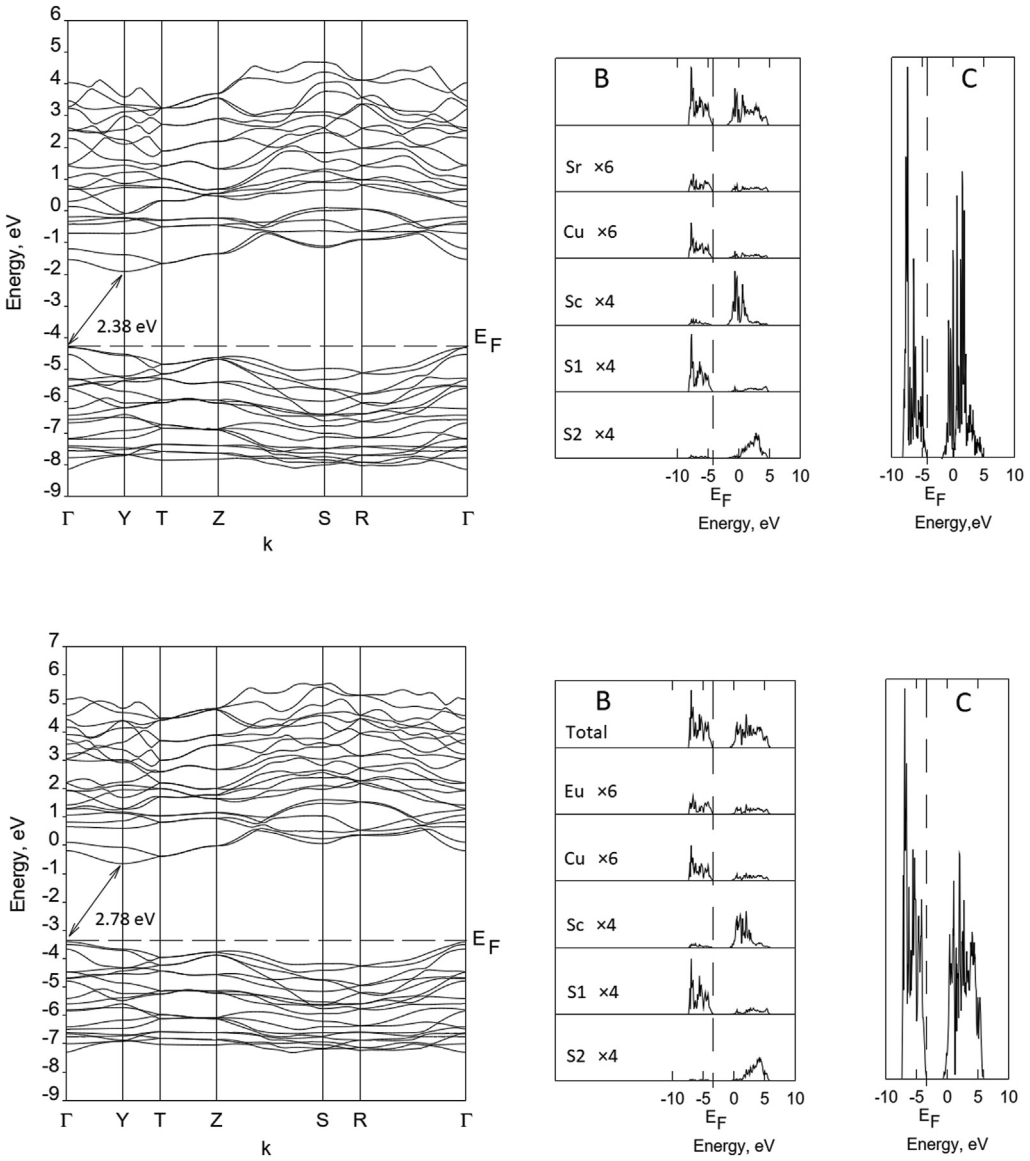

Fig. 7. $SrScCuS_3$ (top) and $EuScCuS_3$ (bottom) band structure and the density of states.

3.3. Raman spectroscopy

The factor-group analysis of the structure of $EuScCuS_3$ and $SrScCuS_3$ crystals was performed to find the symmetries of modes using the local symmetry of all the atomic positions (Table 3). The crystals belong to space group *Cmcm* (№ 63) and their point group is D_{2h} (mmm). The mechanical representation consists of 36 modes. Three modes with B_{1u}, B_{2u} and B_{3u} symmetry are acoustical. The 15 Raman active modes include 5 modes of A_g symmetry, 5 modes of B_{3g} symmetry, 4 modes of B_{1g} symmetry and B_{2g} mode. The infrared active modes include 6 B_{1u}, 6 B_{2u} and 4 B_{3u} symmetry modes (acoustic modes not included). According to the group-theoretical analysis, scandium atoms in position 4a do not participate in the Raman process. The Raman modes observed below 150 cm^{-1} are lattice vibrations. All atoms, except scandium, take part in these vibrations. This interpretation is consistent with the calculation (Table S4). The modes above 150 cm^{-1} are the vibrations of atom groups or individual atoms. The interpretation of the vibrations is shown in Fig. 5. The band in the region from 400 to 460 cm^{-1} (Fig. 5b) is attributed to the presence of SrS impurity in the sample of $SrScCuS_3$. The low-intensity vibrations detected at ~ 472 cm^{-1} were previously observed in Cu_2S compound [64]. We attribute the appearance of 470 and 471 modes to Cu and S vibrations (see Table 2).

3.4. Electronic structure calculations and bandgap measurement

The band structure and the density of states obtained in terms of DFT with the B3LYP functional are shown in Fig. 6. The path in the Brillouin zone is plotted through the highly symmetric points for the orthorhombic lattice. The path is made through Γ-Y-T-Z-S-R-Γ. The coordinates of points are (0,0,0), (1/2,1/2,0), (1/2,1/2,1/2), (0,0,1/2), (0,1/2,0), (0,1/2,1/2) and (0,0,0), respectively. Bilbao Crystallographic Server was used. The band gaps are calculated to be 2.38 eV in $SrScCuS_3$ and 2.78 eV in $EuScCuS_3$. The band gap was defined as the energy difference between the valence band top and conduction band bottom ("HOMO-LUMO" gap). The bandgap is indirect. The calculation was carried out for the ideal crystal structure. The *f*-orbitals of europium were replaced by a pseudopotential.

The measured and calculated Infrared spectra are shown in Fig. 6. The modes in infrared spectra below 170 cm^{-1} are lattice vibrations according to calculations (Fig. 4 and Table S3).

DOS projected onto the whole set of atomic orbitals of Sr (Eu), Cu, Sc and S atoms were calculated near bandgap (Fig. 7, picture C). According to the calculations, the sulfur DOS locate near to the valence band top and conduction band bottom. The strontium (europium) and copper DOS locate near the valence band top. The scandium DOS locate near the

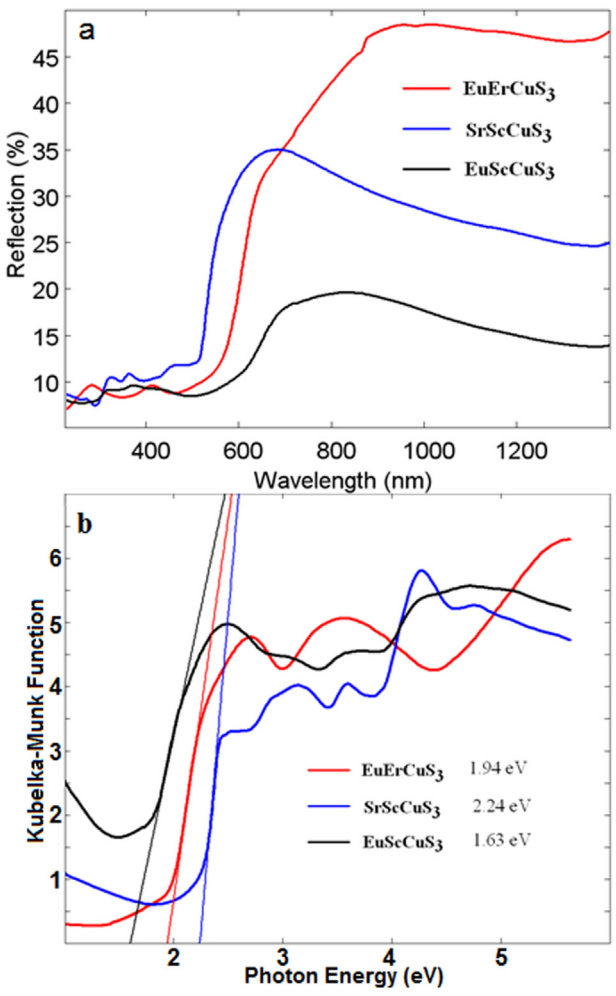

Fig. 8. a) Reflection spectra of $SrScCuS_3$, $EuScCuS_3$ and $EuErCuS_3$. b) Related Kubelka-Munk functions.

conduction band bottom. Thus, $SrScCuS_3$ and $EuScCuS_3$ are midgap, indirect-bandgap semiconductors.

The reflection spectra of $SrScCuS_3$ and $EuScCuS_3$ are presented in Fig. 8a in comparison with that of recently investigated $EuErCuS_3$ [61]. The corresponding Kubelka-Munk functions are given in Fig. 8b. The feature of the reflectance spectra of new scandium-based sulfides is the reduced reflectivity in near-infrared in comparison with $EuErCuS_3$. This implies the presence of the absorption in the infrared that must be absent according to the band structure calculations of ideal crystal structures presented above. This additional infrared absorption must be associated with defects of crystal structure that often take place in sulfides, for instance, in CIGS and CZTS. Specifically, in CZTS these defects are shown to be primarily Cu_{Zn} antisites [65]. In the case of scandium-based sulfides, it is not easy to suggest possible analogous kinds of defects in view of strongly differing radii of all three cations. The nature of these defects needs for a special study. Evidently, they would be harmful in the case of photovoltaic applications of new sulfides, like that in the case of CZTS. Oppositely, the presence of infrared absorption can be useful for thermoelectric applications.

From the Kubelka-Munk plots (Fig. 8b), the band gap values are equal to 2.24 eV for $SrScCuS_3$ and 1.63 eV for $EuScCuS_3$. The first value is in fair agreement with that obtained by the band structure calculations, while, for $EuScCuS_3$, the large discrepancy is observed. Evidently, this discrepancy is due to the imperfect description of Eu^{2+} *4f* orbitals by the pseudopotential used in the calculations. Therefore, the conduction band bottom (or, more correctly, LUMO states) in $EuScCuS_3$ originates from 5*d* orbitals of Eu^{2+} ion. One may note that the experimental value of the bandgap for $EuScCuS_3$ is rather close to the optimal value recommended for photovoltaic materials [66].

The position of the maximum of IR absorption of suspected defects can be accessed through the measurement of their average activation energy. The temperature dependence of electrical resistance *R(T)* of $EuScCuS_3$ sample is shown in Fig. 9(a). The inset of Fig. 9 (a) represents the voltage-current characteristic. Both curves demonstrate typical semiconducting behavior; namely, resistance increases exponentially with cooling. It means charge carriers freezing out or, in other words, thermal activation type of conductivity. From the Arrhenius plot (Fig. 9b), we can estimate activation energy needed to excite carriers from some energy levels to the valence band. The slope of the $\ln R$ $(1/T)$ curve multiplied by Boltzmann constant gives the activation energy E_A. The experimental EA is equal to 0.29 eV that is significantly lower than both DFT-calculated and optically estimated bandgaps.

Consequently, we can suppose that the energy of an additional level extracted from transport properties measurement can be associated with an in-bandgap energy level. Such levels can be formed by defects of the crystal structure. It is highly likely that these levels can lie 0.29 eV above the valence band top and produce hole type carriers in the valence band upon heating. Then, the absorption in the near IR is due to electron transitions from the valence band to these defect levels.

3.5. Thermal properties

In the inert atmosphere, the compounds $AScCuS_3$ (A = Eu, Sr) are thermally stable up to 1520 K. The polymorphic transformations were not detected by the differential scanning calorimetry DSC method over the temperature range of 420–1690 K. On the thermal curves, we detected two-by-two high-temperature endothermal effects reproduced

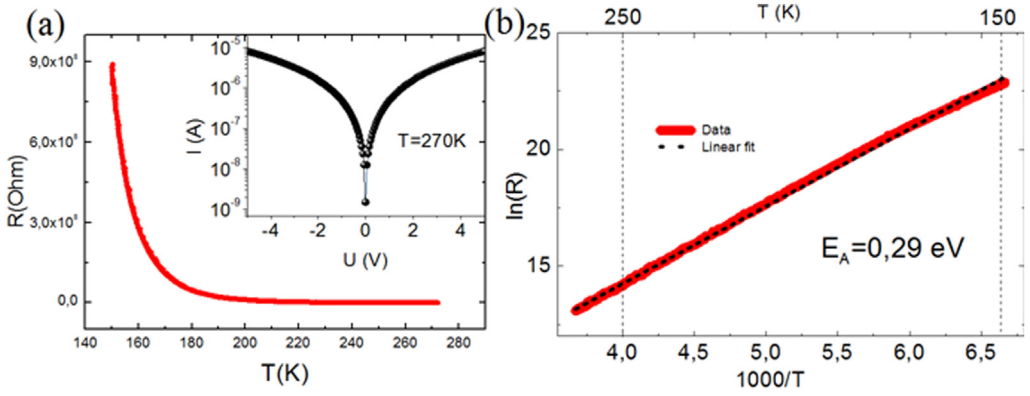

Fig. 9. $EuScCuS_3$ transport properties. a) Temperature dependence of electrical resistance *R(T)*. Inset shows the I–V characteristic. b) Arrhenius plot for activation energy estimation.

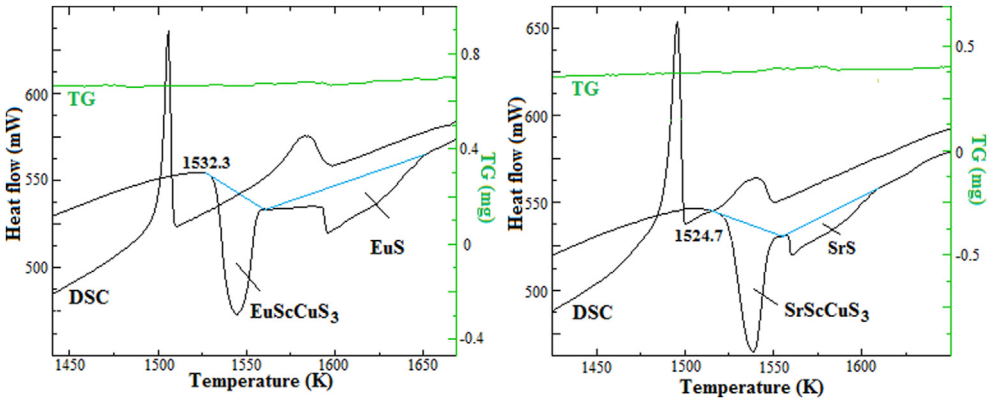

Fig. 10. DSC curves (black) and TG curves (green) of the compounds $AScCuS_3$ (A = Sr, Eu). (For interpretation of the references to colour in this figure legend, the reader is referred to the Web version of this article.)

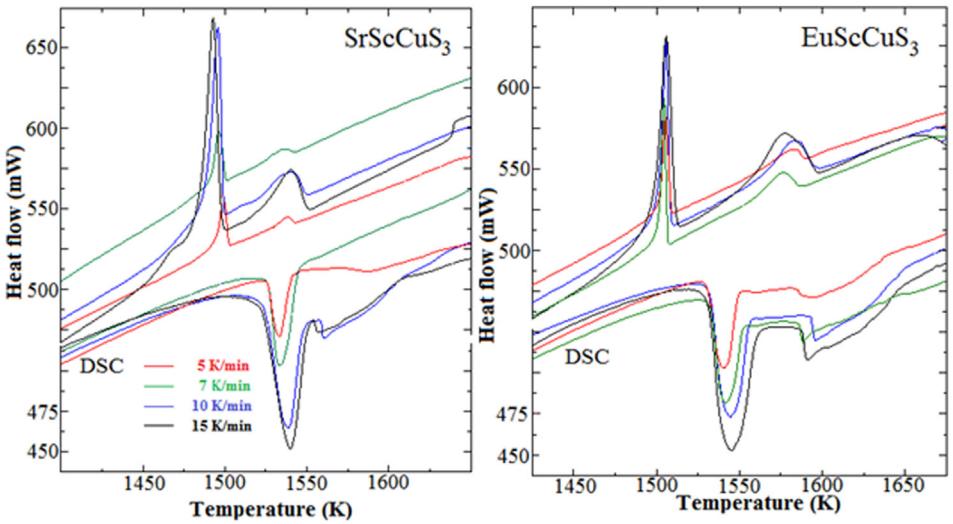

Fig. 11. DSC curves of the compounds $AScCuS_3$ registered under a variety of rates.

on cooling (Fig. 10). The first pick is attributed to incongruent melting of the compounds: T_m = 1524.5 ± 3 K, ΔH_m = 21.6 ± 2.4 kJ•mol^{-1} ($SrScCuS_3$) and T_m = 1531.6 ± 1 K, ΔH_m = 26.1 ± 1.8 kJ•mol^{-1} ($EuScCuS_3$), and the second thermal effect is related tp melting of the primary crystals SrS (ΔH_m = 4.0 ± 0.7 kJ•mol^{-1}) or EuS (ΔH_m = 8.9 ± 0.3 kJ•mol^{-1}) respectively.

The order of obtained temperature values and enthalpies is consistent with the values obtained earlier for isomorphic compounds $SrNdCuS_3$ (T_m = 1429 K, ΔH_m = 16.8 [67]), $EuLaCuS_3$ (T_m = 1539 K, ΔH_m = 23.3 kJ•mol^{-1} [68]), and $BaPrCuS_3$ (T_m = 1580.9 K, ΔH_m = 86.6 kJ•mol^{-1} [31]). Phase transformation is going on according to the scheme $AScCuS_3$ → AS + liq. The values of temperatures and melting enthalpies are deduced from the melting curves. In contrast, the values of the cooling curves were not accounted since the superfusion effect was observed, i.e., the crystallization temperature values are lower than the melting temperatures. The kinetic parameters of incongruent melting of the compounds $AScCuS_3$ (A = Eu, Sr), calculated from the formula of Kissinger [69–71] on the base of the DSC data (Fig. 11) registered under a variety of rates, are presented in Table 4.

The wider thermal effects of the melting process of $EuScCuS_3$ in comparison to $SrScCuS_3$ are indicative of higher value of the activation energy of this process for $EuScCuS_3$, which is in congruence with the calculations performed. The compound $EuScCuS_3$ is kinetically more stable in the inert atmosphere than $SrScCuS_3$ that correlates to the data of temperatures and melting enthalpies of the compounds. Lower stability of $SrScCuS_3$ as compared to $EuScCuS_3$ is probably associated with higher ionicity and higher bonding distance of Sr–S. In the $SrScCuS_3$ structure formed mainly by the ionic polyhedron SrS_6, as well as by the less ionic polyhedra CuS_4 and ScS_6, their mutual inconsistency is likely to occur. In $EuScCuS_3$, three transition metals present and the chemical bonds are less ionic, but relatively more stable, and the MS_n polyhedra are seamlessly associated with the structure that results in higher stability. High values of activation energy indicate the kinetic complexity of the processes of incongruent melting of $AScCuS_3$ compounds occurring at higher

Table 4
Values of the kinetic parameters of the incongruent melting process of the compounds $AScCuS_3$ (A = Eu, Sr).

Compound	$T_{max\ pick}$, K at different rates of heating of the samples				A	E_a, kJ·mol^{-1}
	5 K·min^{-1}	7 K·min^{-1}	10 K·min^{-1}	15 K·min^{-1}		
$EuScCuS_3$	1540.2	1541.1	1543.8	1544.7	$1.72 \cdot 10^{152}$	4545
$SrScCuS_3$	1533.2	1533.5	1538.2	1539.8	$1.56 \cdot 10^{98}$	2941

temperatures than the melting of sesquisulfides and indicate the kinetic inertia of the compounds.

3.6. Magnetic properties

The reciprocal magnetic susceptibility of $EuScCuS_3$ sample rises linearly (Fig. S1) with a temperature above 10 K and it is in very good accordance with Curie-Weiss law (eq. (4)):

$$\chi^{-1} = C^{-1}(T - \theta_W) \quad (2)$$

Fitting of this χ^{-1}-T plot gives 10.2 kmol·m^{-3} K^{-1} for C^{-1} and 6.38 K for θ_W. From this C value, one can calculate effective magnetic moment $\mu_{eff} = 7.91\mu_B$, which is close to the theoretical $7.94\mu_B$ for Eu^{2+} ion. Hence, magnetic properties of $EuScCuS_3$ are defined by ferromagnetic interaction of Eu^{2+} ions. Similar behavior and parameters had been previously observed and calculated in Ref. [72] for $EuLaCuS_3$ and $EuSmCuS_3$ (Table S6). This similarity is because Sc^{3+} like La^{3+} has zero magnetic moment, and the moment of Sm^{3+} is almost ten times smaller than that of Eu^{2+}.

Ions with non-zero magnetic moment are not included in the composition of $SrScCuS_3$; therefore, its magnetic properties are defined by the ratio of diamagnetism of the ion cores and paramagnetism of the valence electrons. The experiment indicates the resulting diamagnetism $\chi \sim -1{\cdot}10^{-9}$ m^3·mol^{-1} at RT.

4. Conclusion

This contribution addresses the synthesis, structure, magnetic, optical and thermal properties of new sulfides $AScCuS_3$ (A = Sr, Eu). The compounds crystallize in a $KZrCuS_3$-type structure, which is typical for the $EuLnCuS_3$ (Ln = Tm-Lu) and $SrLnCuS_3$ (Ln = Er-Lu) compounds. $EuScCuS_3$ experiences a ferromagnetic transition at about 6 K, its melting temperature is 1531.6 K, and optical band gap was found to be 1.63 eV from diffuse reflectance spectrum. The experimental value of the bandgap of $EuScCuS_3$ is rather close to the optimal value recommended for photovoltaic materials. $SrScCuS_3$ is a diamagnetic material; its melting temperature is 1524.5 K, optical band gap is found to be 2.24 eV $AScCuS_3$ is a mid-gap, indirect-bandgap semiconductor. The difference in the optical band gaps of $SrScCuS_3$ and $EuScCuS_3$ is due to the presence of Eu^{2+}*5d* states at the bottom of the conduction band of the latter compound. This demonstrates the possibility of efficient control of the optical band gaps of multication chalcogenides by the inclusion of Eu into their chemical content. Ab initio crystal structure and phonon spectrum calculations have been performed for $SrScCuS_3$ and $EuScCuS_3$ in terms of the LCAO-MO approach and density functional theory with the use of the B3LYP hybrid functional. The results of the calculations make it possible to interpret the observed vibrational spectra.

CRediT authorship contribution statement

Anna V. Ruseikina: Conceptualization, Writing - original draft, Writing - review & editing, Formal analysis, of results and writing the manuscript, thermal measurements and interpretation, corresponding author, All authors reviewed and commented on the manuscript. **Maxim S. Molokeev:** Writing - original draft, Writing - review & editing, structural measurements and interpretation, paper writing, . **Vladimir A. Chernyshev:** Writing - original draft, Writing - review & editing, accomplishment of the DFT calculations, paper writing, . **Aleksandr S. Aleksandrovsky:** reviewed and commented on the manuscript, reviewed and commented on the manuscript, Writing - review & editing, Formal analysis, Writing - original draft, analysis of results and writing the manuscript. Interpretation of optical data and data on transport properties., , reviewed and commented on the manuscript. **Alexander S. Krylov:** Writing - review & editing, measurement of Raman spectra, . **Svetlana N. Krylova:** Writing - original draft, Writing - review & editing, Formal analysis, analysis of Raman spectra, paper writing, . **Dmitriy A. Velikanov:** Writing - review & editing, magnetic measurements, . **Maxim V. Grigoriev:** Writing - original draft, Writing - review & editing, samples synthesis, sample preparation for all physical measurements, SEM interpretation, paper writing, . **Nikolai G. Maximov:** Writing - review & editing, measurement of reflection spectra, . **Nikolai P. Shestakov:** Writing - review & editing, measurement of IR . **Alexander A. Garmonov:** Writing - original draft, Writing - review & editing, interpretation of magnetic properties, paper writing, . **Alexey V. Matigorov:** Writing - review & editing, sample preparation for magnetic metering, . **Anton S. Tarasov:** Writing - review & editing, Formal analysis, Data curation, analysis of transport data, . **Mikhail V. Rautskii:** Writing - review & editing, measurement of transport properties, . **Nikolai A. Khritokhin:** Writing - review & editing, determination of kinetic parameters of the compound decomposition processes, . **Ludmila V. Melnikova:** Writing - original draft, Writing - review & editing, paper writing, linguistic and editorial revision, . **Nikolay Yu Tretyakov:** Writing - review & editing, SEM measurements, .

Declaration of competing interest

The authors declare that they have no known competing financial interests or personal relationships that could have appeared to influence the work reported in this paper.

Acknowledgements

The work was supported by the Ministry of Science and Higher Education of the Russian Federation under Project No. FEUZ-2020-0054; by RFBR Grant 18-02-00754; by the "UMNIK" program research project № 14977GY/2019; by the Ministry of Science and Higher Education of the Russian Federation (contract no. 05.594.21.0019, unique identification number RFMEFI59420X0019). Maxim S. Molokeev, Anton S. Tarasov and Mikhail V. Rautskii acknowledge additional funding from Research Grant No. 075-15-2019-1886 from the Government of the Russian Federation. The subset research was performed in Research Resource Center "Natural Resource Management and Physico-Chemical Research." The use of equipment of Krasnoyarsk Regional Center of Research Equipment of Federal Research Center « Krasnoyarsk Science Center SB RAS» is acknowledged.

Appendix A. Supplementary data

Supplementary data to this article can be found online at https://doi.org/10.1016/j.jssc.2020.121926.

References

[1] D.O. Scanlon, G.W. Watson, Stability, geometry, and electronic structure of an alternative I-III-VI_2 material, $CuScS_2$: a hybrid density functional theory analysis, Appl. Phys. Lett. 97 (2010), 131904, https://doi.org/10.1063/1.3491179.
[2] J.P. Dismukes, R.T. Smith, J.G. White, Physical properties and crystal structure of a new semiconducting I–III–VI2 compound, CuScS2, J. Phys. Chem. Solid. 32 (1971) 913–922, https://doi.org/10.1016/S0022-3697(71)80336-0.
[3] S.B. Zhang, S.H. Wei, A. Zunger, H. Katayama-Yoshida, Defect physics of the $CuInSe_2$ chalcopyrite semiconductor, Phys. Rev. B 57 (1998) 9642–9656, https://doi.org/10.1103/PhysRevB.57.9642.
[4] A.J. Nelson, A.M. Gabor, M.A. Contreras, J.R. Tuttle, R. Noufi, P.E. Sobol, K.G. Lynn, Comparison of polycrystalline $Cu(In,Ga)Se_2$ device efficiency with junction depth and interfacial structure, J. Appl. Phys. 78 (1995) 269–272, https://doi.org/10.1063/1.360669.

[5] A.M. Gabor, J.R. Tuttle, D.S. Albin, M.A. Contreras, R. Noufi, A.M. Hermann, High-efficiency $CuIn_xGa_{1-x}Se_2$ solar cells made from $(In_x,Ga_{1-x})_2Se_3$ precursor films, Appl. Phys. Lett. 65 (1994) 198–200, https://doi.org/10.1063/1.112670.

[6] S.-H. Wei, S.B. Zhang, A. Zunger, Effects of Ga addition to $CuInSe_2$ on its electronic, structural, and defect properties, Appl. Phys. Lett. 72 (1998) 3199–3201, https://doi.org/10.1063/1.121548.

[7] I.G. Austin, C.H.L. Goodman, A.E.J. Pengelly, New semiconductors with the chalcopyrite structure electrochem, J. Electrochem. Soc. 103 (1956) 609. https://iopscience.iop.org/article/10.1149/1.2430171/pdf. (Accessed 25 June 2020).

[8] I. Repins, M. Contreras, M. Romero, Y. Yan, W. Metzger, J. Li, S. Johnston, B. Egaas, C. DeHart, J. Scharf, Characterization of 19.9%-Efficient CIGS, 33rd IEEE Photovoltaic Specialists Conference, San Diego, June, 2008. Paper NREL/CP-520-42539.

[9] M.A. Contreras, K. Ramanathan, J. AbuShama, F. Hasoon, D.L. Young, B. Egaas, R. Noufi, Diode characteristics in state-of-the-art ZnO/CdS/Cu(In1-xGax)Se_2 solar cells, Prog. Photovoltaics Res. Appl. 13 (2005) 209–216, https://doi.org/10.1002/pip.626.

[10] I.L. Repins, B.J. Stanbery, D.L. Young, S.S. Li, W.K. Metzger, C.L. Perkins, W.N. Shafarman, M.E. Beck, L. Chen, V.K. Kapur, D. Tarrant, M.D. Gonzalez, D.G. Jensen, T.J. Anderson, X. Wang, L.L. Kerr, B. Keyes, S. Asher, A. Delahoy, B. von Roedern, Comparison of device performance and measured transport parameters in widely varying Cu(In,Ga)(Se,S) solar cells, Prog. Photovoltaics Res. Appl. 14 (2006) 25–43, https://doi.org/10.1002/pip.654.

[11] L.D. Gulay, V.Ya Shemet, I.D. Olekseyuk, Crystal structures of the compounds YCuS2, Y3CuSnS7 and YCuPbS3, J. Alloys Compd. 388 (2005) 59–64, https://doi.org/10.1016/j.jallcom.2004.06.074.

[12] J.P. Dismukes, J.G. White, The preparation, properties, and crystal structures of some scandium sulfides in the range Sc_2S_3-ScS, Inorg. Chem. 3 (1964) 1220–1228, https://doi.org/10.1021/ic50019a004.

[13] G.B. Jin, E.S. Choi, T.E. Albrecht-Schmitt, Syntheses, structures, magnetism, and optical properties of gadolinium scandium chalcogenides, J. Solid State Chem. 182 (2009) 1075–1081, https://doi.org/10.1016/j.jssc.2009.02.002.

[14] H. Matsushita, T. Maeda, A. Katsui, T. Takizawa, Thermal analysis and synthesis from the melts of Cu-based quaternary compounds Cu–III–IV–VI_4 and Cu_2–II–IV–VI_4 (II = Zn, Cd; III = Ga, In; IV = Ge, Sn; VI = Se), J. Cryst. Growth 208 (2000) 416–422, https://doi.org/10.1016/s0022-0248(99)00468-6.

[15] Y.M. Andreev, V.V. Atuchin, G.V. Lanskii, N.V. Pervukhina, V.V. Popov, N.C. Trocenco, Linear optical properties of $LiIn(S1\text{-}x_{Sex})(_2)$ crystals and tuning of phase matching conditions, Solid State Sci. 7 (10) (2005) 1188–1193, https://doi.org/10.1016/j.solidstatesciences.2005.05.005.

[16] T.J. Wang, Z.H. Kang, H.Z.Z. hang, Z.S. Feng, F.G. Wu, H.Y. Zang, Y. Jiang, J.Y. Gao, Y. Andreev, G. Lanskii, Sellmeier equations for green, yellow, and orange colored $HgGa_2S_4$ crystals, Appl. Phys. Lett. 90 (18) (2007), 181913, https://doi.org/10.1063/1.2734923.

[17] Z.S. Feng, Z.H. Kang, F.G. Wu, J.Y. Gao, Y. Jiang, H.Z. Zhang, Y.M. Andreev, G.V. Lanskii, V.V. Atuchin, T.A. Gavrilova Shg, Doped GaSe: in crystals, Optic Express 16 (13) (2008) 9978–9985, https://doi.org/10.1364/OE.16.009978.

[18] A.H. Reshak, V.V. Atuchin, S. Auluck, I.V. Kityk, First and second harmonic generation of the optical susceptibilities for the non-centro-symmetric orthorhombic $AgCd_2GaS_4$, J. Phys. Condens. Matter 20 (32) (2008) 352234, https://doi.org/10.1088/0953-8984/20/32/325234.

[19] V.P. Sachanyuk, G.P. Gorgut, V.V. Atuchin, I.D. Olekseyuk, O.V. Parasyuk, The Ag_2S-In_2S_3-Si(Ge)S_2 systems and crystal structure of quaternary sulfides $Ag_2In_2Si(Ge)S_6$, J. Alloys Compd. 452 (2) (2008) 348–358, https://doi.org/10.1016/j.jallcom.2006.11.043.

[20] P. Wu, A.E. Christuk, J.A. Ibers, New quaternary chalcogenides $BaLnMQ_3$ (Ln = rare earth or Sc; M = Cu, Ag; Q=S, Se), structure and property variation vs rare-earth element, J. Solid State Chem. 110 (1994) 337–344, https://doi.org/10.1006/jssc.1994.1177.

[21] M. Eberle, T. Schleid, Expanding the $SrCuRES_3$ series with the rare-earth metals scandium and yttrium, in: 24th Annual Conference of the German Crystallographic Society, Stuttgart, March, 2016. https://books.google.ru/books?id=klu7CwAAQBAJ&pg=PT237&dq=SrCuScS. (Accessed 25 June 2020).

[22] H.M. Pathan, J.D. Desai, C.D. Lokhande, Modified chemical deposition and physico-chemical properties of copper sulphide (Cu_2S) thin films, Appl. Surf. Sci. 202 (2002) 47–56, https://doi.org/10.1016/S0169-4332(02)00843-7.

[23] D. Perniu, S. Vouwzee, A. Dutta, J. Schoonman, Defect chemistry of solar cell chalcopyrite materials, J. Optoelectron. Adv. Mater. 9 (2007) 1568.

[24] N.V. Sikerina, Regularities of Phase Equilibria in SrS-Ln_2S_3-Cu_2S Systems, Preparation and Structure of $SrLnCuS_3$ Compounds, Ph.D. Dissertation, University of Tyumen, Tyumen, 2005, https://elib.utmn.ru/jspui/bitstream/ru-tsu/2441/1/472.pdf. (Accessed 25 June 2020).

[25] N.O. Azarapin, T.M. Burkhanova, A.V. Solovyova, Synthesis and Optical Properties of $BaPrCuS_3$, 16th International Scientific Conference-School “Materials of Nano-, Micro-optoelectronics and Fiber Optics. Physical Properties and Application”, Saransk, September, 2017. http://bibl.laser.nsc.ru/download/Abstracts_VNKSH_2017.pdf. (Accessed 25 June 2020).

[26] R.L. Blaine, H.E. Kissinger, Homer kissinger and the kissinger equation, Thermochim. Acta 450 (2012) 1–6, https://doi.org/10.1016/j.tca.2012.04.008.

[27] V.A. Kochedigov, I.D. Zakiryanova, I.V. Korzun, Research of thermal dissociation of interaction products of rare-earth element oxides with the components of atmospheric air, Analytica and Control 9 (2005) 58–63. http://elar.urfu.ru/bitstream/10995/58914/1/aik-2005-01-08.pdf. (Accessed 25 June 2020).

[28] G.A. Hussen, D.J. Buttrey, P. DeSanto, A.A. Abd-Elgaber, H. Roshdy, Myhoud Ali, Formation and characterization of samarium oxide generated from different precursors, Thermochim. Acta 402 (2003) 27–36, https://doi.org/10.1016/S0040-6031(02)00535-X.

[29] L. Paama, I. Pitkanen, H. Halttunen, P. Peramamaki, Ifrared evolved gas analysis during thermal investigation of lanthanium, eurpian and samarium carbonates, Thermochim. Acta 403 (2003) 197–206, https://doi.org/10.1016/S0040-6031(03)00038-8.

[30] Quick reference handbook of physio-chemical values 7nd ed.; eds. K. P. Mischenko, A. A. Ravdel; Chemistry, Leningrad, 1974, 100. https://docplayer.ru/383745-Kratkiy-spravochnik-fiziko-himicheskih-velichin.html (accessed 25 June 2020).

[31] N.O. Azarapin, A.S. Aleksandrovsky, V.V. Atuchin, T.A. Gavrilova, A.S. Krylov, M.S. Molokeev, Sh Mukherjee, A.S. Oreshonkov, O.V. Andreev, Synthesis, structural and spectroscopic properties of orthorhombic compounds $BaLnCuS_3$ (Ln = Pr, Sm), J. Alloys Compd. 832 (2020) 153134, https://doi.org/10.1016/j.jallcom.2019.153134.

[32] J.W. Visser, A fully automatic program for finding the unit cell from powder data, J. Appl. Crystallogr. 2 (1969) 89–95, https://doi.org/10.1107/S0021889869006649.

[33] Bruker AXS TOPAS V4: General Profile and Structure Analysis Software for Powder Diffraction Data. – User’s Manual, Bruker AXS, Karlsruhe, Germany, 2008.

[34] N.V. Sikerina, O.V. Andreev, Crystal structures of $SrLnCuS_3$ (Ln= Gd, Lu), Russ. J. Inorg. Chem. 52 (2007) 581–584, https://doi.org/10.1134/S0036023607040183.

[35] A.V. Ruseikina, L.A. Solovyov, M.V. Grigoriev, O.V. Andreev, Crystal structure variations in the series $SrLnCuS_3$ (Ln = La, Pr, Sm, Gd, Er and Lu), Acta Crystallogr. C: Struct. Chem. C75 (2019) 584–588, https://doi.org/10.1107/S2053229619004984.

[36] W.T. Pennington, Diamond – visual crystal structure information system, J. Appl. Crystallogr. 32 (1999) 1028–1029.

[37] V.G. Tsirelson, Quantum Chemistry. Molecules, Molecular Systems and Solids, third ed., Binom, Knowledge Lab, Moscow, 2014.

[38] A.D. Becke, Density-functional thermochemistry. III. The role of exact exchange, J. Chem. Phys. 98 (1993) 5648–5652, https://doi.org/10.1063/1.464913.

[39] P.L. Stephens, F.J. Devlin, C.F. Chabalowski, M.J. Frisch, Ab initio calculation of vibrational absorption and circular dichroism spectra using density functional force fields, J. Phys. Chem. 98 (1994) 11623–11627, https://doi.org/10.1021/j100096a001.

[40] R. Dovesi, V.R. Saunders, C. Roetti, R. Orlando, C.M. Zicovich-Wilson, F. Pascale, B. Civalleri, K. Doll, N.M. Harrison, I.J. Bush, Ph D’Arco, M. Llunel, M. Causa, Y. Noel, L. Maschio, A. Erba, M. Rerat, S. Casassa, CRYSTAL17 user’s manual. http://www.crystal.unito.it/Manuals/crystal17.pdf, 2018. (Accessed 25 June 2020).

[41] Crystal. http://www.crystal.unito.it/index.php. (Accessed 20 July 2019).

[42] M. Dolg, H. Stoll, A. Savin, H. Preuss, Energy-adjusted pseudopotentials for the rare earth elements, Theor. Chim. Acta 75 (1989) 173–194, https://doi.org/10.1007/BF00528565.

[43] M. Dolg, H. Stoll, H. Preuss, A combination of quasi relativistic pseudopotential and ligand field calculations for lanthanoid compounds, Theor. Chim. Acta 85 (1993) 441–450, https://doi.org/10.1007/BF01112983.

[44] Energy-consistent pseudopotentials of the stuttgart/cologne group. http://www.tc.uni-koeln.de/PP/clickpse.en.html. (Accessed 29 October 2018).

[45] K. Doll, N.M. Harrison, Chlorine adsorption on the Cu(111) sur54rface, Chem. Phys. Lett. 317 (2000) 282–289, https://doi.org/10.1016/S0009-2614(99)01362-7.

[46] T. Ouazzani, A. Lichanot, C. Pisani, C. Roetti, Relaxation and electronic structure of surfaces in lithium sulphide: a Hartree-Fockab initio approach, J. Phys. Chem. Solid. 54 (1993) 1603–1611, https://doi.org/10.1016/0022-3697(93)90356-V.

[47] M. Kaupp, P.v.R. Schleyer, H. Stoll, H. Preuss, Pseudopotential approaches to Ca, Sr, and Ba hydrides. Why are some alkaline earth MX_2 compounds bent? J. Chem. Phys. 94 (1991) 1360–1366, https://doi.org/10.1063/1.459993.

[48] T. Bredow, K. Jug, R.A. Evarestov, Electronic and magnetic structure of $ScMnO_3$, Phys. Status Solidi (2006) R10–R12, https://doi.org/10.1002/pssb.200541403 (b) 243.

[49] V.A. Chernyshev, A.E. Nikiforov, V.P. Petrov, A.V. Serdtsev, M.A. Kaschenko, S.A. Klimin, Structure and lattice dynamics of rare-earth ferroborate crystals: ab initio calculation, Phys. Solid State 58 (2016) 1642–1650, https://doi.org/10.1134/S1063783416080096.

[50] V.A. Chernyshev, V.P. Petrov, A.E. Nikiforov, Lattice dynamics of rare-earth titanates with the structure of pyrochlore $R_2Ti_2O_7$ (R = Gd, Tb, Dy, Ho, Er, Tm, Yb, and Lu): ab initio calculation, Phys. Solid State 57 (2015) 996–1002, https://doi.org/10.1134/S1063783415050078.

[51] N.V. Volkov, A.S. Tarasov, M.V. Rautskii, A.V. Lukyanenko, I.A. Bondarev, S.N. Varnakov, S.G. Ovchinnikov, Magneto-transport phenomena in metal/SiO_2/n(p)-Si hybrid structures, J. Magn. Magn Mater. 451 (2018) 143–158, https://doi.org/10.1016/j.jmmm.2017.11.008.

[52] R.L. Blaine, H.E. Kissinger, Homer kissinger and the kissinger equation, Thermochim. Acta 450 (2012) 1–6, https://doi.org/10.1016/j.tca.2012.04.008.

[53] D.A. Velikanov, Magnetometer with a superconducting quantum interferometric sensor, RF Pat., 2481591. http://www.freepatent.ru/patents/2481591, 2013. (Accessed 19 October 2020).

[54] D.A. Velikanov, Vibration magnetometer, RF pat., 2341810. http://www.freepatent.ru/patents/2341810, 2008. (Accessed 19 October 2020).

[55] R.D. Shannon, Revised effective ionic radii and systematic studies of interatomic distances in halides and chalcogenides, Acta Crystallogr. A 32 (1976) 751–767, https://doi.org/10.1107/S0567739476001551.

[56] A.V. Ruseikina, O.V. Andreev, Regularities of change in the structural parameters of $EuLnCuS_3$ (Ln = La–Nd, Sm, Gd, Ho), Russ. J. Inorg. Chem. 62 (2017) 160–167, https://doi.org/10.1134/S0036023617020140.

[57] N. Grinvud, A. Ernsho, The Chemistry of Elements, Binom, Laboratoriyaznanii, Moscow, 2008.
[58] L.A. Koscielski, J.A. Ibers, The structural chemistry of quaternary chalcogenides of the type AMM'Q_3, Z. Anorg. Allg. Chem. 638 (2012) 2585–2593, https://doi.org/10.1002/zaac.201200301.
[59] M. Wakeshima, F. Furuuchi, Y. Hinatsu, Crystal structures and magnetic properties of novel rare-earth copper sulfides, $EuRCuS_3$ (R = Y, Gd–Lu), J. Phys. Condens. Matter 16 (2004) 5503–5518, https://doi.org/10.1088/0953-8984/16/30/012.
[60] F. Furuuchi, M. Wakeshima, Y. Hinatsu, Magnetic properties and (151) Eu Mossbauer effects of mixed valence europium copper sulfide Eu_2CuS_3, J. Solid State Chem. 177 (2004) 3853–3858, https://doi.org/10.1016/j.jssc.2004.04.034.
[61] A.V. Ruseikina, L.A. Solovyov, V.A. Chernyshev, A.S. Aleksandrovsky, O.V. Andreev, S.N. Krylova, A.S. Krylov, D.A. Velikanov, M.S. Molokeev, N.G. Maximov, M.V. Grigoriev, A.A. Garmonov, A.V. Matigorov, Synthesis, structure, and properties of $EuErCuS_3$, J. Alloys Compd. 805 (2019) 779–788, https://doi.org/10.1016/j.jallcom.2019.07.059.
[62] I.D. Brown, D. Altermatt, Bond-valence parameters obtained from a systematic analysis of the inorganic crystal structure database, Acta Crystallogr. Sect. B Struct. Sci. 41 (1985) 244–247, https://doi.org/10.1107/S0108768185002063.
[63] S. Bell, Measurement Good Practice Guide, National Physical Laboratory, Teddington, Middlesex, 2001.
[64] C. Lai, Q. Wu, J. Chen, L. W, Sh Ren, Large-area aligned branched Cu_2S nanostructure arrays: room-temperature synthesis and growth mechanism, Nanotechnology 21 (2010), 215602, https://doi.org/10.1088/0957-4484/21/21/215602.
[65] S. Chen, Ji-H. Yang, X.G. Gong, A. Walsh, Su-H. Wei, Intrinsic point defects and complexes in the quaternary kesterite semiconductor Cu_2ZnSnS_4, Phys. Rev. B 81 (2010), 245204, https://doi.org/10.1103/PhysRevB.81.245204.
[66] A.S. Oreshonkov, E.M. Roginskii, V.V. Atuchin, New candidate to reach Shockley-Queisser limit: the DFT study of orthorhombic silicon allotrope Si(oP32), J. Phys. Chem. Solid. 137 (2020), 109219, https://doi.org/10.1016/j.jpcs.2019.109219.
[67] A.V. Ruseikina, O.V. Andreev, E.O. Galenko, S.I. Koltsov, Trends in thermodynamic parameters of phase transitions of lanthanide sulfides $SrLnCuS_3$ (Ln=La-Lu), J. Therm. Anal. Calorim. 128 (2017) 993–999, https://doi.org/10.1007/s10973-016-6010-9.
[68] A.V. Ruseikina, O.V. Andreev, Phase equilibria in the Cu_2S–La_2S_3–EuS system, Russ. J. Inorg. Chem. 62 (2017) 610–618, https://doi.org/10.1134/S0036023617050199.
[69] N. Bukovec, P. Bukovec, J. Šiftar, Kinetics of the thermal decomposition of $Pr_2(SO_4)_3$ to $Pr_2O_2SO_4$, Thermochim. Acta 35 (1) (1980) 85–91, https://doi.org/10.1016/0040-6031(80)85025-8.
[70] A.S. Lyadov, V.V. Kurilkin, Reduction specifics of rare-earth orthovanadates (ReE = La, Nd, Sm, Dy, Ho, Er, Tm, Yb, and Lu), Russ. J. Inorg. Chem. 61 (2016) 86–92, https://doi.org/10.1134/S0036023616010150.
[71] J. Llopiz, M.M. Romero, A. Jerez, Y. Laureiro, Generalization of the kissinger equation for several kinetic models, Thermochim. Acta 256 (1995) 205–211, https://doi.org/10.1016/0040-6031(94)02109-2.
[72] A.V. Ruseikina, D.A. Velikanov, A.A. Garmonov, M.V. Grigoriev, A.Ye Pinigina, V.V. Balashov, Magnetic Properties of the Compounds $EuLnCuS_3$ (Ln = La, Ce, Nd, Sm, Ho), the IIId All-Russian Conference Hot Spots of Solid State Chemistry: from New Ideas to Innovative Materials, Novosibirsk, October, 2019.